Earth-Science Reviews 226 (2022) 103955

Contents lists available at ScienceDirect

Earth-Science Reviews

journal homepage: www.elsevier.com/locate/earscirev

Incipient ocean spreading beneath the Arabian shield

Irina M. Artemieva [a,b,c,d,*], Haibin Yang [e], Hans Thybo [a,c,f]

[a] SinoProbe Laboratory, Chinese Academy of Geological Sciences, Beijing 100037, China
[b] Marine Geodynamics, GEOMAR Helmholtz Center for Ocean Research, Kiel 24148, Germany
[c] State Key Laboratory GPMR, School of Earth Sciences, China University of Geosciences, Wuhan 430074, China
[d] Department of Geophysics, Stanford University, Stanford, CA 94305, USA
[e] Research School of Earth Sciences, Australian National University, Canberra 0200, Australia
[f] Eurasia Institute of Earth Science, Istanbul Technical University, Istanbul 34469, Turkey

A B S T R A C T

Formation of new oceans by continental break-up is understood as a continuous evolution from rifting to ocean spreading. The Red Sea is one of few locations on Earth where a new plate boundary presently forms. Its evolution provides key information on how the plate tectonics operates and how the plate boundaries form and evolve in time. While the new plate boundary has already been formed in the southern Red Sea where ocean spreading is active, the north-central segment still experiences continental rifting. The region also has west-east asymmetry: in the north-central Red Sea the rift-related magmatism is not located beneath the rift axis, as conventional models predict, but instead is offset by ca 300 km into Arabia.

We propose a new geodynamic model which explains the enigmatic asymmetry of the Red Sea region and is fully consistent with various types of geological and geophysical observations. We demonstrate that the north-central rift is a transient feature that will not develop into coincident ocean spreading. Instead, the new plate boundary forms across Arabia. Our numerical experiments, supported by geological, seismic and gravity observations, predict that in 1–5 Myr the north-central extensional axis will jump ~300 km eastward into Arabia. The Ad Damm strike-slip fault, normal to the central Red Sea rift axis, will evolve into a transform fault between the on-going ocean spreading in the southern Red Sea and the future spreading in north-central Arabia.

We demonstrate that crustal-scale weakness zones control lithosphere extension and lead to long-distance jumps of extensional axes in continental lithosphere not affected by hotspots. Therefore, our model also provides theoretical basis for understanding dynamics and mechanisms of the transition from rifting to continental break-up at passive continental margins not affected by hotspots.

1. Introduction

Formation of new oceans is a fundamental plate tectonic process that produces new lithosphere plates. Extension in continental lithosphere causes rifting, which may continue into continental breakup and ocean spreading (Kendall et al., 2005; Lizarralde et al., 2007; Huismans and Beaumont, 2011; Wright et al., 2012; Liao and Gerya, 2015). These processes are primarily controlled by the dynamic interplay of far-field stresses caused by plate reorganizations and lithosphere weakening associated with mantle convective instabilities. The dynamics of rift-to-drift evolution depends on rheological coupling in the lithosphere (Liao and Gerya, 2015), rift obliquity (Corti, 2008), erosion/sedimentation (Bialas and Buck, 2009), mantle lithosphere depletion (Lizarralde et al., 2007), hotspot magmatism (Ebinger and Casey, 2001; Kendall et al., 2005; Bastow et al., 2011), lithosphere weakness zones (Liao and Gerya, 2015) and crustal-scale faults (Yang et al., 2018; Molnar et al., 2020). Rifts often fail without leading to continental breakup. However, it is commonly assumed that ocean spreading already active in the southern Red Sea will develop northward into the present continental rift in the central-northern Red Sea (Ghebreab, 1998; Cochran, 2005; Almalki et al., 2015; Augustin et al., 2021; El Khrepy et al., 2021).

Ocean spreading may also fail and the spreading axis may jump. Hotspot magmatic heating close to mid-ocean ridges is proposed as the dominant cause of ridge jumps in mature oceans with typical ridge relocation of <100 km distance (Mittelstaedt et al., 2008). On-shore, jumps of extensional axes at the initial stages of ocean opening have yet been reported only for Iceland (Wright et al., 2012), which is located above a hotspot and where it is uncertain if the lithosphere is continental or oceanic. Thus, the fundamental problem of possible long-distance extensional jumps in continental lithosphere has not yet been addressed and, consequently, this process has not been included to plate paleo-reconstructions.

Here we demonstrate by numerical experiments that under certain conditions (1) the extensional axis may jump over hundreds of kilometres in cratonic lithosphere and (2) this process does not require hotspot presence. The importance of our discovery is that this proposed

* Corresponding author at: SinoProbe Laboratory, Chinese Academy of Geological Sciences, Beijing 100037, China
E-mail address: iartemieva@geomar.de (I.M. Artemieva).

https://doi.org/10.1016/j.earscirev.2022.103955
Received 10 August 2021; Received in revised form 15 January 2022; Accepted 27 January 2022
Available online 2 February 2022

process is now in operation in the Red Sea region, such that the numerical model can be tested by geophysical and geological observations.

2. Models of the Red Sea evolution

The formation of the Red Sea-Ethiopian rift-Gulf of Aden triple divergent junction above a mantle plume may have triggered continental break-up (Burke and Dewey, 1973; Courtillot, 1982). Combined with a large volume of continental flood basalts in the region, this hypothesis led to the commonly accepted view that lithosphere rupturing and volcanism in the Red Sea-Afar region was associated with mantle plume(s) (Ebinger and Sleep, 1998; Park et al., 2007; Chang et al., 2011; Bosworth et al., 2016; Koptev et al., 2018). Alternatively, a part of or all rifting was attributed to far-field forces (Voggenreiter et al., 1988; McGuire and Bohannon, 1989), e.g. associated with the Mediterranean subduction systems (Reilinger and McClusky, 2011) or slab pull caused by subduction of the Arabian plate beneath Zagros (McQuarrie et al., 2003; Yao et al., 2017) (Fig. 1)..

2.1. Along-strike variations: continental rifting vs ocean spreading

The Red Sea formed at 24 ± 4 Ma by continental rifting along the Nubia–Somalia–Arabia plate boundaries, which began at ~30 Ma following extension in the Gulf of Aden, and evolved into ocean spreading in the southern Red Sea at ~12–13 Ma (Izzeldin, 1987; Augustin et al., 2021), although the oldest recognizable magnetic anomaly corresponds to 4.18 Ma and the oldest identified oceanic crust (at ~17 ^{o}N, 40.5°E) is of the early Pleistocene age (4.62 Ma) (Izzeldin, 1987; Schettino et al., 2016). Yet the absence of marine rift-parallel magnetic anomalies north of ~20–22 ^{o}N (Coleman and McGuire, 1988; Cochran, 2005; Schettino et al., 2016) indicates that oceanic crust does not yet form in the central-northern part of the Red Sea (Fig. 2).

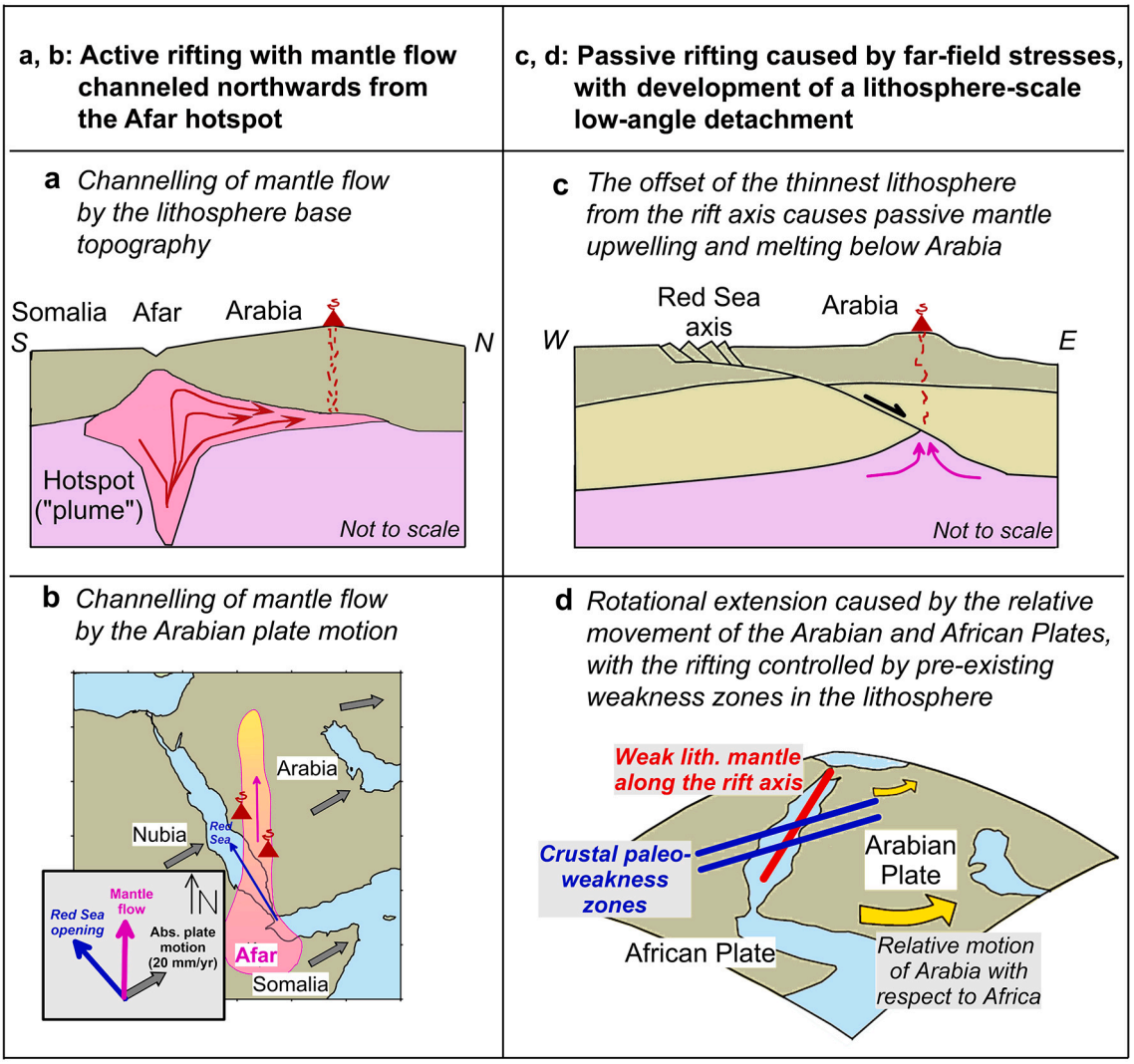

Fig. 1. Schematic end-member models proposed for the Red Sea – Arabian Shield late Cenozoic evolution. (a-b) Active rifting with mantle flow channelled northwards from the Afar hotspot (Camp and Roobol, 1992; Park et al., 2007; Al-Saud, 2008; Yao et al., 2017), e.g. (a) by the LAB topography (Hansen et al., 2007; Petrunin et al., 2020) or (b) by the Arabian plate motion (Hansen et al., 2006; Park et al., 2007; Chang et al., 2011; Elsheikh et al., 2014); absolute plate velocity is based on (ArRajehi et al., 2010). (c-d) Passive rifting caused by far-field stresses, with possible development of a lithosphere-scale low-angle detachment (c) (Voggenreiter et al., 1988; McGuire and Bohannon, 1989; Yao et al., 2017). Far-field forces are either associated with the separation of Arabia from Africa (Makris and Rihm, 1991; Bosworth et al., 2016; Molnar et al., 2020), driven by Neotethys Mediterranean subduction systems (Reilinger and McClusky, 2011), or subduction of the Arabian plate beneath Zagros (McQuarrie et al., 2003; Yao et al., 2017). The offset of the thinnest lithosphere from the rift axis causes passive mantle upwelling and melting below Arabia. (d) Rotational extension caused by relative movement of the Arabian Plate with respect to the African Plate during the Nubia-Arabia divergence. Pre-existing weakness zones in the lithosphere, especially along the Red Sea axis, control the evolution of rifting (Molnar et al., 2020). (For interpretation of the references to colour in this figure legend, the reader is referred to the web version of this article.)

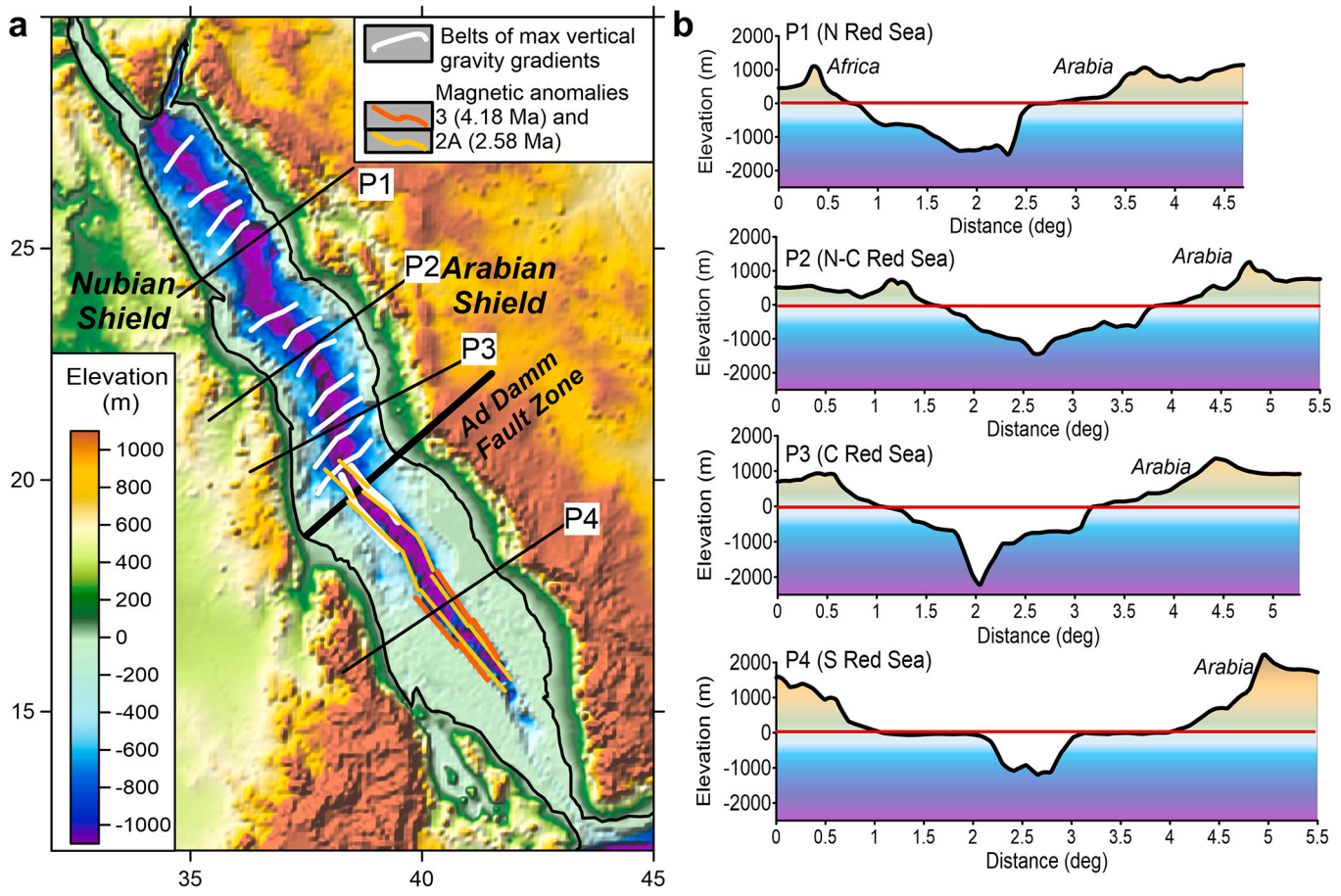

Fig. 2. (a) Topography of the Red Sea region. White lines – belts of the maximal values of the vertical gravity gradient (Augustin et al., 2021); the belts are perpendicular to the extensional axis north of ~20°N and are axis-parallel south of the Ad Damm strike-slip fault. The fault (thick black line, Zahran et al., 2019) separates the two domains with the contrasting styles of lithosphere deformation as also refelected in the Red Sea bathymetry. Orange lines in the southern Red Sea show the oldest recognizable magnetic anomaly 3; yellow lines mark magnetic isochron 2A (based on Schettino et al., 2016). Marine rift-parallel magnetic anomalies are absent north of ~20–22 °N and south of ~15 °N (Coleman and McGuire, 1988; Cochran, 2005; Schettino et al., 2016). (b) Topographic profiles across the Red Sea. Locations are marked in (a). (For interpretation of the references to colour in this figure legend, the reader is referred to the web version of this article.)

This conventional view supported by regional seismic, gravity and magnetic observations has been challenged in two recent studies. One of them (Augustin et al., 2021) interpretes the north-central Red Sea as an ultra-slow spreading center using an analogy with the Mid-Atlantic and Reykjanes Ridges near Iceland and with the Galapagos Spreading Centre, where rift-parallel magnetic and gravity anomalies are absent because of the Iceland and Galapagos hotspots, respectively. However, no hotspot mantle anomaly is known in the north-central Red Sea from regional seismic studies (Park et al., 2007; Chang et al., 2011; Yao et al., 2017; Kaviani et al., 2020) (Fig. 3b). Furthermore, the pattern of vertical gravity gradient (VVG) anomalies in the north-central Red Sea (north of ~20 °N) with the identified series of eleven ridge-perpendicular belts of the maximal VVG values (Augustin et al., 2021) (Fig. 2) cannot be explained by spearding. In contrast, the maximal VVG anomalies are ridge-parallel in the studied part of the southern Red Sea between ~20 and 17°N (Augustin et al., 2021), where the ridge-parallel magnetic anomalies associated with the ocean spreading are also observed (Schettino et al., 2016) (Fig. 2). Therefore, the pattern of the VVG anomalies with a ~90° angle between the spreading axis and the belts of the maximal VVG values is consistent with melt flow normal to the rift axis in the north-central Red Sea, rather then with ocean spreading.

The other study that challenged the conventional view on the continental rifting in the northern Red Sea (El Khrepy et al., 2021) hypothesizes that the north-central (around ~25 °N) Red Sea region may be at the transitional stage to ocean spreading based on a regional tomography model, which resolved a typical continental rift in the northernmost part (~26–27 °N) but has neither lateral nor vertical resolution below the north-central Red Sea basin south of 26 °N (see the Supplementary Information in El Khrepy et al., 2021). We note that all other seismic models image thin (<15 km), oceanic-type, crust (Fig. 3a) and low-velocity upper mantle (Fig. 3b) only in the southern Red Sea basin (Chang et al., 2011; Kaviani et al., 2020).

The different styles of the lithosphere deformation in the southern and north-central parts of the Red Sea are consistent with the strikingly different bathymetry, with a narrow deep valley in the south and a broad depression north of ~20 °N (Fig. 2). A combination of active rifting associated with the Afar plume in the south and passive rifting in the north was proposed to explain a sharp difference in the structure of the southern and northern parts of the Red Sea (Chang et al., 2011; Petrunin et al., 2020). These models imply that the northern Red Sea rifting will continue and may evolve into seafloor spreading (Ghebreab, 1998; Cochran, 2005; Augustin et al., 2021; El Khrepy et al., 2021). However, scenarios with a ceased rifting have not yet been examined.

2.2. *Across-strike variations: West Arabia magmatic province*

Red Sea rifting was associated with massive alkali basaltic volcanism in the south with a peak at ~30 Ma in Ethiopia and at 30–26 Ma in SW Arabia (Yemen) (Kendall et al., 2005; Wolfenden et al., 2005; Bastow et al., 2011). In the north-central Red Sea region all rift-related <10 Ma

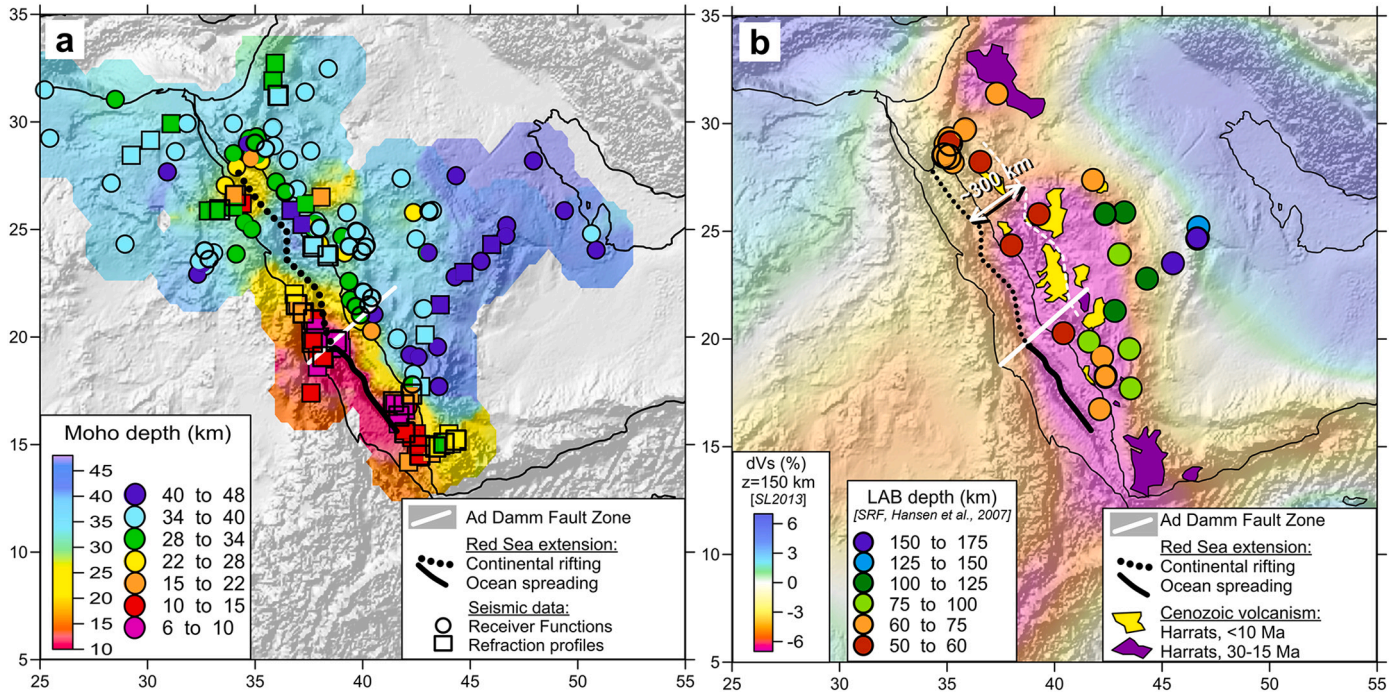

Fig. 3. (a) Interpolated seismic Moho depth (superimposed on a shaded relief) in the Arabian and Nubian shields and the Red Sea. Colour symbols – Moho depth based on receiver functions (Sandvol et al., 1998; Hansen et al., 2007; Al-Damegh et al., 2004; Hosny and Nyblade, 2016; Tang et al., 2016) and refraction profiles (Makris et al., 1983; Mooney et al., 1985; Mechie et al., 1986; El-Isa et al., 1987; Badri, 1990; Egloff et al., 1991; Makris and Rihm, 1991; Mechie et al., 2013). (b) Depth to the lithosphere base (LAB) based on S-receiver functions (colour circles) (Hansen et al., 2007) superimposed on Vs anomalies at 150 km depth (Schaeffer and Lebedev, 2013) and a shaded relief. White dashed line ~300 km eastward from the Red Sea axial zone follows the line of <10 Ma harrats. The Red Sea axial zone is marked by black dots in the north-central part with continental rifting and by black line in the southern part with ocean spreading. White line – the Ad Damm strike-slip fault (Zahran et al., 2019) that marks the transition from ocean spreading to rifting. (For interpretation of the references to colour in this figure legend, the reader is referred to the web version of this article.)

magmatic complexes (harrats) are displaced by 200–400 km from the Red Sea axis into Arabia (Figs. 4, 5a), and an enigmatic observation is an apparent gap in western Arabia volcanism at ca. 20–10 Ma (Fig. 5b), which was explained by far-field plate-boundary forces (Courtillot, 1982; Bosworth et al., 2016). We speculate that the two distinct pulses of volcanism may alternatively be associated with the along-rift difference in the style of the Red Sea extension: in general the boundary between the young and old harrats spatially correlates with the N extent of the ocean spreading zone (Figs. 4-5).

The prominent west-east asymmetry of the north-central Red Sea rift-related magmatism is marked by an associated >1500 km long belt of negative Bouguer anomalies (Fig. 6a) and low seismic velocities in the upper mantle of western Arabia (Figs. 3a, 5a), which suggests the presence of low-density, high-temperature mantle material (Benoit et al., 2003; Chang et al., 2011; Koulakov et al., 2016; Yao et al., 2017). Yet normal thickness of the mantle transition zone beneath the Arabian shield (Benoit et al., 2003) indicates that the temperature anomaly has shallow origin. The 100–300 km wide negative Bouguer anomaly belt implies that the centre of mass of the low-density material is located at ~50–80 km depth, consistent with typical depths of basaltic magma generation by decompressional melting (McKenzie and Bickle, 1988) and with the presence of a thin (50–75 km) lithosphere beneath western Arabia (Hansen et al., 2007) (Fig. 3b).

Despite differences between geodynamic models, they commonly assume that the West Arabia continental flood basalts (CFB) province was formed by melt generation beneath the southern Red Sea axial zone (Camp and Roobol, 1992; Park et al., 2007; Chang et al., 2011). The across-strike asymmetry of the north-central Red Sea in seismic and gravity anomalies is commonly explained by the melt channelized by upper mantle flow from the Afar hotspot northward to western Arabia (Chang et al., 2011; Petrunin et al., 2020) (Fig. 1b). This hypothesis is challenged by observations. Mantle flow channelling is consistent with the almost N-S fast polarization of shear-waves in western Arabia (Elsheikh et al., 2014) which, however, does not match the present absolute plate motion (Fig. 6b). At the same time, fossil anisotropy cannot explain consistent delay times between the fast and slow waves at all stations in the region with a highly variable lithosphere thickness (Elsheikh et al., 2014). Furthermore, northward mantle flow is inconsistent with fault geometry, deformation pattern, and focal plane solutions for earthquakes at Lunayyir harrat (ca 25 ^{o}N, 37 °E) (Fig. 6b) which are better explained by asthenospheric flow perpendicular to the Red Sea rift axis (Pallister et al., 2010). These observations suggest that melt generation is associated not with the Afar plume, but with the extension in the rift zone, from where melt is channelled eastwards to the western Arabia magmatic province. Such interpretation is consistent with the axis-perpendicular belts of high vertical gravity gradients in the north-central Red Sea (Augustin et al., 2021) (Fig. 2a).

Alternatively, geological models favour passive rifting, in which lithosphere extension is attributed to far-field forces of various origin (Yao et al., 2017; Voggenreiter et al., 1988; Makris and Rihm, 1991) (Fig. 1cd). The across-strike north-central Red Sea asymmetry is explained by a low-angle lithosphere-scale detachment fault formed during the Red Sea rifting (Voggenreiter et al., 1988) which causes eastward displacement of the decompressional melting zone from the rift axis into Arabia. However, the along strike differences between the northern and southern parts of the Red Sea region cannot be explained by these models.

3. Setup of numerical experiments

We perform numerical experiments to explain the asymmetries of the southern and north-central Red Sea by a single, consistent geodynamic

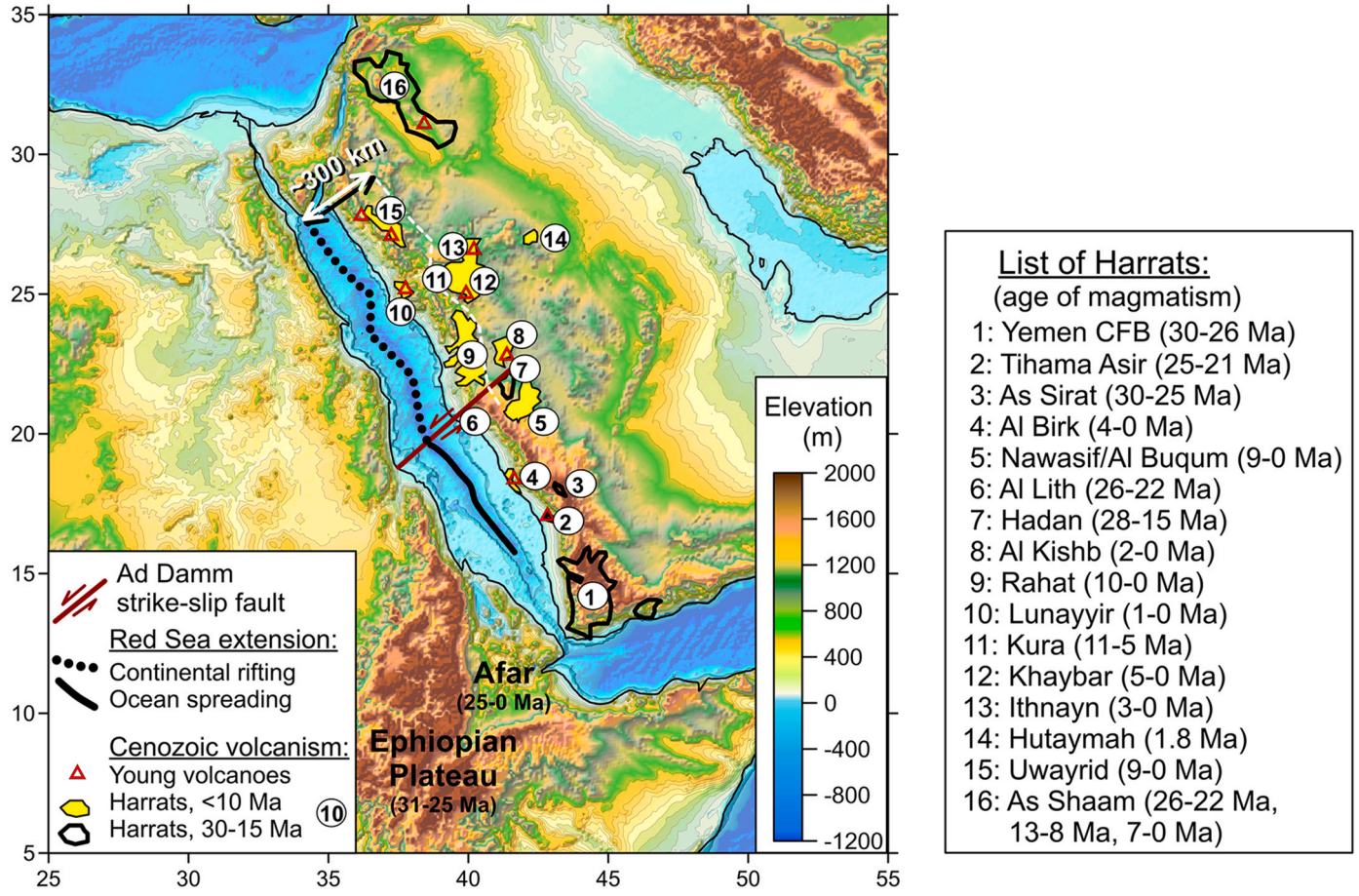

Fig. 4. Topography and volcanism in Arabia (Camp et al., 1991). Volcanism in Africa is not shown. White dashed line ~300 km eastward from the Red Sea axial zone follows the line of <10 Ma harrats. The transition from ocean spreading (black line) to continental rifting (black dots) in the Red Sea roughly corresponds to the Ad Damm strike-slip fault (dark red line) (Zahran et al., 2019). (For interpretation of the references to colour in this figure legend, the reader is referred to the web version of this article.)

model and to predict future lithosphere deformation in the region. To be consistent with various geophysical and geological observations, geodynamic models for the Red Sea evolution should explain the following:

(1) the west-east asymmetry of geophysical upper mantle models in the north-central segment, (Figs. 3b, 5b, 6);

(2) the along-strike asymmetry with seafloor spreading in the south and continental rifting in the north, where the axis-parallel magnetic anomalies are absent in the absence of an upper mantle hotspot anomaly (Figs. 2, 3a);

(3) the north-south change, from 30 -20 Ma magmatism close to the present oceanic spreading in the south, to <10 Ma magmatism displaced by ~300 km from the present continental rift in the north-central Red Sea (Figs. 4-5);

(4) a ca 10 Myr long gap in western Arabia magmatism (Fig. 5b);

(5) preferential vertical mantle flow in the south and horizontal mantle flow normal to the rift axis in the north (Figs. 5a, 6b);

(6) axis-perpendicular alignment of the maximal vertical gravity gradients north of ~20°N and their axis-parallel orientation south of the Ad Damm fault (Fig. 2a).

We adopt the hypothesis that the western Arabia Cenozoic volcanic province is associated with passive rifting of the north-central Red Sea caused by far-field forces, which reactivated lithosphere weakness zone along a ca. 600 Ma (Pan-African) Red Sea suture between the Nubian and Arabian cratons (Makris and Rihm, 1991). We propose that the location of this pre-extensional crustal weakness zone relative to a change in lithosphere thickness across the Red Sea controls the style of deformation and location of magmatism. Our approach builds on geological, geophysical and numerical studies that demonstrate a major role of pre-existing crustal weakness zone in lithosphere deformation during rifting (Dunbar and Sawyer, 1988; Morley, 1989; KRISP Working Party, 1991; Van Wijk, 2005; Buck, 2007; Cloetingh et al., 2013; Bonini et al., 2015; Deng et al., 2017; Yang et al., 2018; Osagiede et al., 2021).

We use the 2D finite element code Underworld2 (Moresi et al., 2007) to model thermo-mechanical deformation of the crust and upper mantle with visco-plastic, non-Newtonian rheologies during lithosphere extension in the presence of decompressional adiabatic mantle melting (for details see Appendix A). More than 1 million randomly distributed Lagrangian markers are used to track the history of material properties, e.g. density, viscosity and melt fraction. Our regional model, which simulates deformation of the crust and upper mantle in the presence of a pre-existing crustal-scale weakness zone, leads to continental rift development and incipient ocean spreading. While the evolution of the Red Sea is inherently 3D, our 2D model predicts and successfully explains all known geological and geophysical observations.

We adopt a typical structure of the initial cratonic lithosphere with the LAB (lithosphere-asthenosphere boundary) depth of 200 km in the Nubian shield and 140 km in the Neoproterozoic Arabian shield (Artemieva and Mooney, 2001). The Nubian and Arabian shields are separated by a transitional zone (model distance km 150–300) where the Moho and the LAB depth are linearly interpolated between the two cratons (Fig. A1, Tables A1-A2). Within the transitional zone we introduce a 6 km wide, E-dipping, crust-cutting weakness zone. We apply a constant extensional velocity of 12 mm/yr, which corresponds to the rate of the Red Sea opening in the central segment at ca. 20–24°N

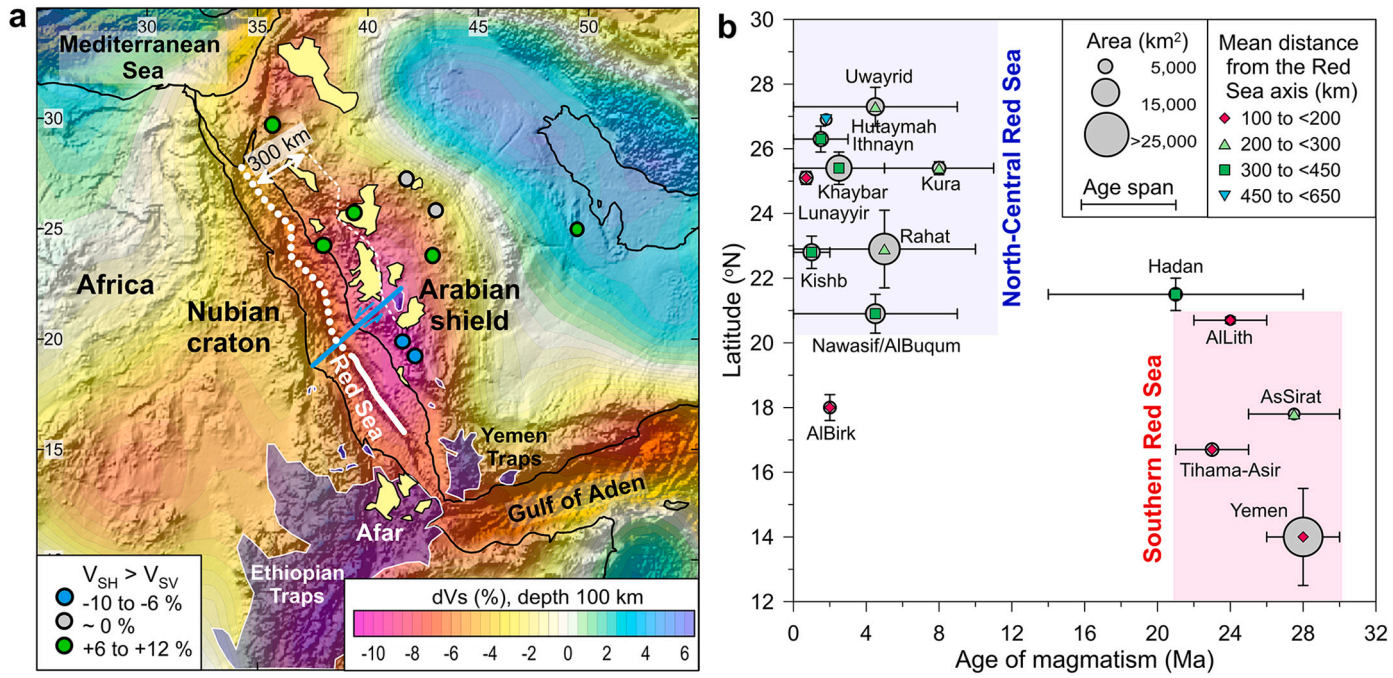

Fig. 5. Geophysical and geological observations in the Red Sea – Arabian Shield region. (a) Seismic Vs anomalies at 100 km depth (Schaeffer and Lebedev, 2013) superimposed on a shaded relief. Colour circles – mantle transverse anisotropy (Tkalčić et al., 2006), negative/positive values correspond to vertical/horizontal mantle flow (see also Fig. 6b). Shaded areas - Cenozoic volcanism (Camp and Roobol, 1992) (purple 30–20 Myr, yellow 10–0 Myr). White dashed line 300 km eastward from the Red Sea axis follows central line of young harrats. The Red Sea axial zone is marked by white dots for continental rifting and white line for ocean spreading. Blue line - the Ad Damm strike-slip fault (Zahran et al., 2019) between the two domains with different styles of lithosphere deformation. (b) Age of magmatism, latitude, areal size, and distance from the Red Sea extensional axis for western Arabia harrats (for locations see Fig. 4). (For interpretation of the references to colour in this figure legend, the reader is referred to the web version of this article.)

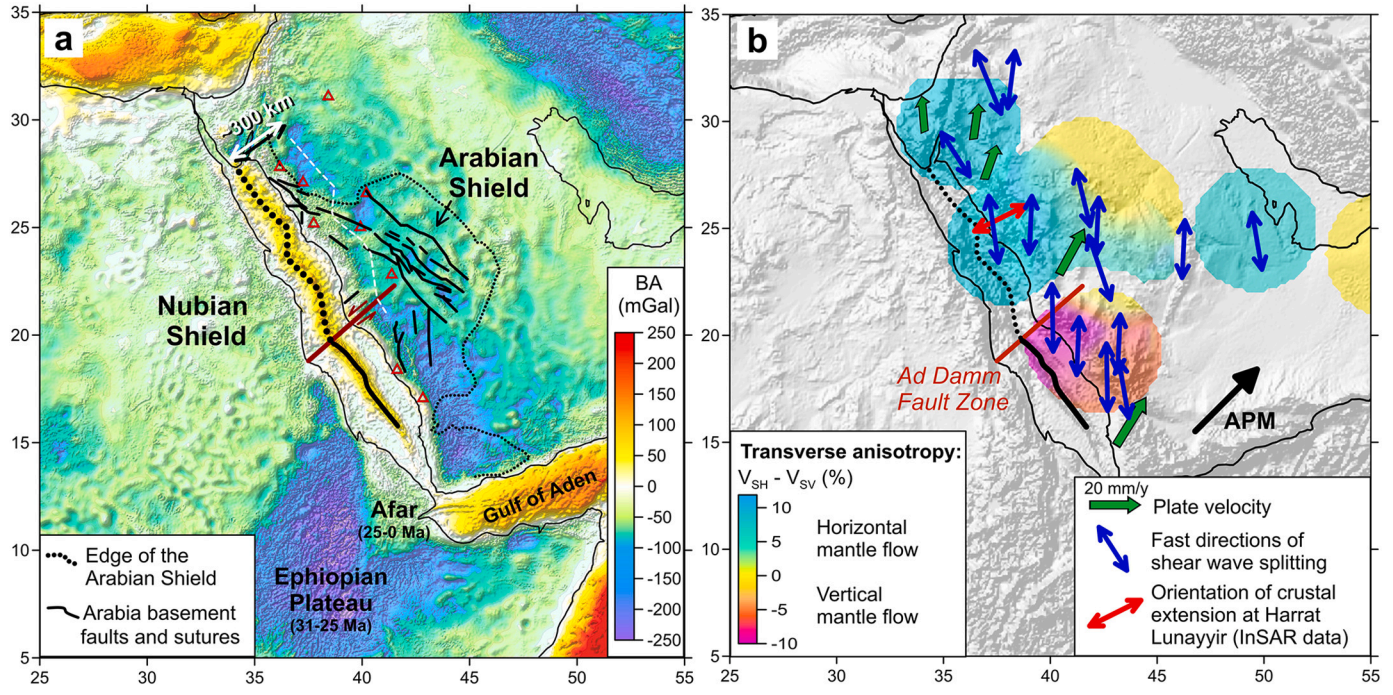

Fig. 6. Geophysical and geological observations in the Red Sea – Arabian Shield region (background – shaded relief). (a) Bouguer anomalies; thin dotted black line – outline of the Arabian shield; thin black lines – major faults in the Precambrian basement (after Johnson et al., 2011). White dashed line 300 km eastward from the Red Sea axis generally follows central line of young harrats. The Red Sea axial zone is marked by black dots for continental rifting and black line for ocean spreading. Dark red line - the Ad Damm strike-slip fault (Zahran et al., 2019) between the two domains with different styles of lithosphere deformation. (b) Crustal and mantle deformation styles. Background colors - mantle transverse anisotropy (interpolation based on (Tkalčić et al., 2006), see Fig. 5a), blue arrows - fast directions of shear-wave splitting (Hansen et al., 2006), red arrow - direction of a principal tensional axis in the crust at Harrat Lunayyir (Pallister et al., 2010), and green arrows - the Arabian plate velocity (Reilinger and McClusky, 2011). (For interpretation of the references to colour in this figure legend, the reader is referred to the web version of this article.)

(ArRajehi et al., 2010), and demonstrate that the position of the pre-extensional weakness zone controls the lithosphere deformation.

Two model experiments (Figs. 7-8) explain geophysical and geological observations in the southern (Case S) and north-central (Case N) Red Sea region. In Case S, the paleo-weakness zone is located along the margin of the Arabian craton (km 300), while in Case N it is located in the middle of the Nubia-Arabia transition (km 240), i.e. above thicker and stronger lithospheric mantle than in Case S (Fig. A1).

4. Lithosphere extension in the southern Red Sea

Case S (Fig. 7) evolves as a classic rift-to-drift model with lithosphere thinning and decompressional mantle melting at the rift axis which evolves into seafloor spreading. Our model does not include processes associated with the Afar triple junction, which may contribute to the evolution of the southern Red Sea region, e.g. magmatism in the Yemen continental flood basalt province. The model predicts the following evolution of the southern segment of the Red Sea region.

(1) A low-angle lithosphere-scale detachment fault is formed (Fig. 7a) as proposed by geological data (Voggenreiter et al., 1988).

(2) Lithosphere extension causes eastward migration of the rift axis with a rate of ~10 km/Myr (Fig. 7a-d) until seafloor spreading initiates (Fig. 7e). After ~10 Myr of extension, the pre-extensional weakness zone is abandoned and new spreading forms in the thin lithosphere ~100 km east of the initial rift axis (Fig. 7bb', 9b).

(3) Lithosphere thinning to ~70–100 km initiates decompressional melting and magmatism at the new extensional centre (Fig. 7bc).

(4) The model predicts that after ~15–17 Myr, extension on the detachment fault ceases, thus terminating eastwards displacement of magmatism (Fig. 7d, 9b), and by ~17 Myr magmatism localizes in a < 50 km wide zone (Fig. 7d'e'), as observed at the southern Red Sea oceanic spreading (Figs. 2a,5a).

Model time 17.1 Myr corresponds to the present evolution of the southern Red Sea region (Fig. 7ee'). The model predicts ongoing ocean spreading of the southern Red Sea at the present mid-ocean ridge and accounts for the following observations.

Thin (<15 km) crust at the spreading centre is consistent with formation of oceanic crust in agreement with seismic data (Fig. 3a). Extremely thin (30–50 km) lithosphere around the spreading centre and thicker (~100 km) lithosphere in southern-western Arabia is consistent with seismic S-wave receiver function observations (Hansen et al., 2007) (Fig. 3b). The presence of the upper mantle melt zone at ~40–120 km depth is supported by combined traveltime and waveform inversion (Chang et al., 2011) and Rayleigh wave tomography (Yao et al., 2017). The larger present mantle melting zone in Case S than in Case N (Fig. 8d) is in agreement with the strong negative Bouguer anomaly in the SW part of the Arabian peninsula (Fig. 6a).

5. Lithosphere extension in the north-central Red Sea

Case N (Fig. 8) is a typical model with off-rift magmatism (Yang et al., 2018), where lithosphere thinning and mantle melting are displaced hundreds kilometres from the rift axis. The model predicts all geophysical observations along the north-central segment of the Red Sea rift zone.

(1) At the early stages of extension, a low-angle lithosphere-scale detachment fault forms as observed in geological data (Voggenreiter et al., 1988) (Fig. 8a).

(2) During the first ~10 Myr of extension, the lithosphere weakens and thins to ~100 km approximately 300 km to the east of the rift axis. However, the deformation is yet insufficient to initiate decompressional mantle melting (Fig. 8ab).

(3) A new weakness zone, displaced far from the extensional axis, forms in the lithospheric mantle (Fig. 8b) and, in contrast to Case S (Fig. 7b), crustal and mantle deformation detach.

(4) Due to the offset of the new mantle weakness zone from the extensional axis (Fig. 8b), magmatism initiated at ~10–12 Myr is displaced eastwards by ~300–350 km from the Red Sea rift axis (Fig. 4-5) to the zone of localized crustal deformation (Fig. 8cd).

(5) The ca. 10 Myr delayed onset of rift-related magmatism in the northern Red Sea since the initiation of lithosphere extension, which started later than in the southern Red Sea, explains the gap in volcanism in western Arabia at 20–10 Ma (Fig. 5b).

The present evolution of the north-central Red Sea region corresponds to model time 13.8 Myr (Fig. 8d), i.e. soon after the onset of magmatism (Fig. 8c) in agreement with dominant ages of the north-central western Arabian harrats (Fig. 4). The model accounts for the following geophysical observations.

The predicted strongly localized crustal thinning to <20 km close to the extensional axis is observed on seismic refraction profiles in the northern Red Sea (Fig. 3a). The numerical experiments do not predict notable crustal thinning beneath the north-central part of western Arabia where the model predicts crustal thickness of 30–35 km below the young (<10 Myr) volcanic fields (Fig. 8cd), in agreement with seismic data (Fig. 3a).

The lithosphere preserves the cratonic thickness (120–150 km) below the north-central Red Sea axial zone, where the structure is unresolved by seismic data (Benoit et al., 2003; Hansen et al., 2007; El Khrepy et al., 2021), but thins significantly (to ~50–80 km) below the young harrats in western Arabia, in agreement with results from S-receiver functions (Hansen et al., 2007) and seismic tomography (Yao et al., 2017; Schaeffer and Lebedev, 2013) (Fig. 3b, 5a).

The numerical experiments predict that deformation at the present rift axis has decreased since the early stages (Fig. 8bd) and that the extension occurs ~250–400 km further east in a broad zone in Arabia as observed in geological studies of faults, seismicity distribution and focal mechanisms (Pallister et al., 2010) (Fig. 9a). In agreement with the Bouguer anomaly (Fig. 6a), the numerical experiments predict that the ~100 km deep mantle melt zone is located directly below the western Arabia volcanic fields ~200–400 km from the rift axis (Fig. 8dd'), as also observed in surface wave tomography (Chang et al., 2011; Yao et al., 2017) (Figs. 3b, 5a).

The model predicts sub-horizontal mantle flow in a broad area between the rift axis and the volcanic fields (Fig. 8d), which is consistent with (a) observed strong (~10%) $V_{SH} > V_{SV}$ polarization anisotropy (Tkalčić et al., 2006) (Figs. 5a, 6b) and (b) observations at Lunayyir harrat (Fig. 6b), where fault geometry, deformation style, and focal plane solutions are explained by asthenospheric flow perpendicular to the Red Sea rift axis (Pallister et al., 2010).

Shear-wave splitting interpretations in western Arabia generally detect fast axes which are sub-parallel to the Red Sea in the north (Fig. 6b). While anisotropy is usually attributed to olivine alignment by channelled mantle flow, shear-wave splitting based on SKS, PKS and similar phases cannot distinguish between anisotropy in the crust and the mantle. The prevailing NW-SE (320^o - 340^o) alignments of volcanic vents, major dykes, lineaments and faults in the north-central part of western Arabia (Camp and Roobol, 1992; Johnson et al., 2011) are all parallel to the Red Sea axis (~330^o) (Zahran et al., 2019) (Fig. 6ab), whereas the fast polarization of shear-waves is parallel to N-S (~0^o) trends of major faults and basement structures in the southern Red Sea region (Fig. 6). Therefore, crustal anisotropy may significantly contribute to the observed shear-wave splitting in the Arabian shield, in analogy with the Kaapvaal craton where strong crustal anisotropy parallel to the strike of major dyke swarms accounts on average for 30–50% of the total SKS splitting (Thybo et al., 2019), which conventionally earlier was explained by mantle flow.

6. Future evolution of the Red Sea

Our major finding is that rifting in the north-central Red Sea is a transient feature which soon will end (Fig. 8e), unless a significant change in the far-field stress may occur. Our model predicts that, during

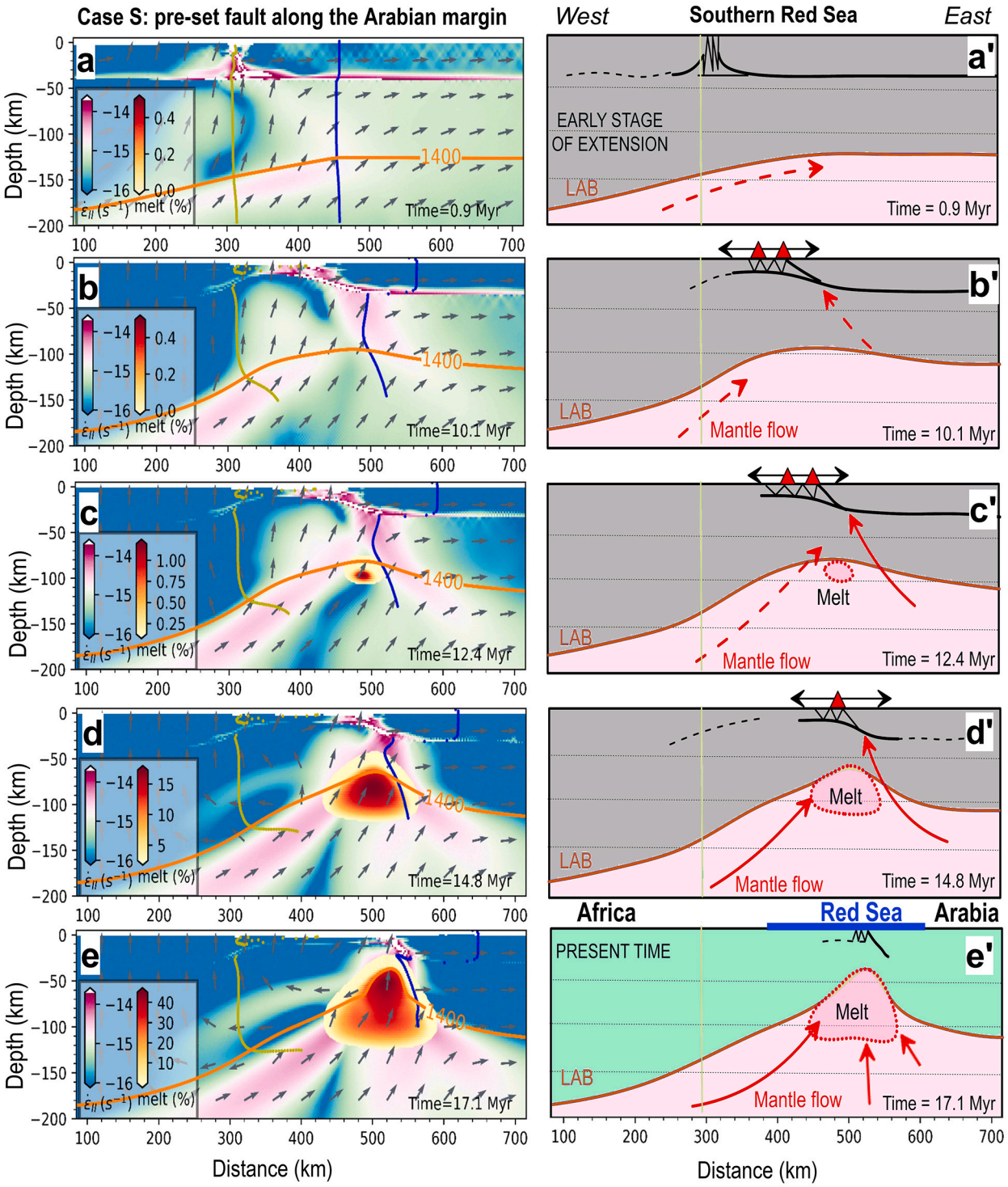

Fig. 7. Case S: Snapshots of strain rate (shown with log10 scale) and melt fraction evolution in the southern Red Sea (left) and line-drawings of major model features (right). Left panels: yellow and blue lines - deformation of initial vertical lines at the pre-set fault (km 300) and at the right end of the LAB ramp (km 450); arrows of uniform length show the material velocity direction; orange lines – 1400 °C isotherm. Right panels: black lines – faults (solid lines – major faults, dashed line – secondary faults); red lines – mantle flow direction; orange lines – lithosphere-asthenoshere boundary (LAB) assumed to be at 1400 °C isotherm; red triangles atop – volcanoes and harrats. (a): A low-angle lithosphere-scale detachment fault formed at an early stage of extension is marked by the zone of high deformation (magenta colors in the left panel and black line in the right panel). (b-c): After ~10 Myr of extension, mantle melting produces a zone of localized magmatism below the rift graben; (d-e): ocean spreading begins after ~15 Myr. (For interpretation of the references to colour in this figure legend, the reader is referred to the web version of this article.)

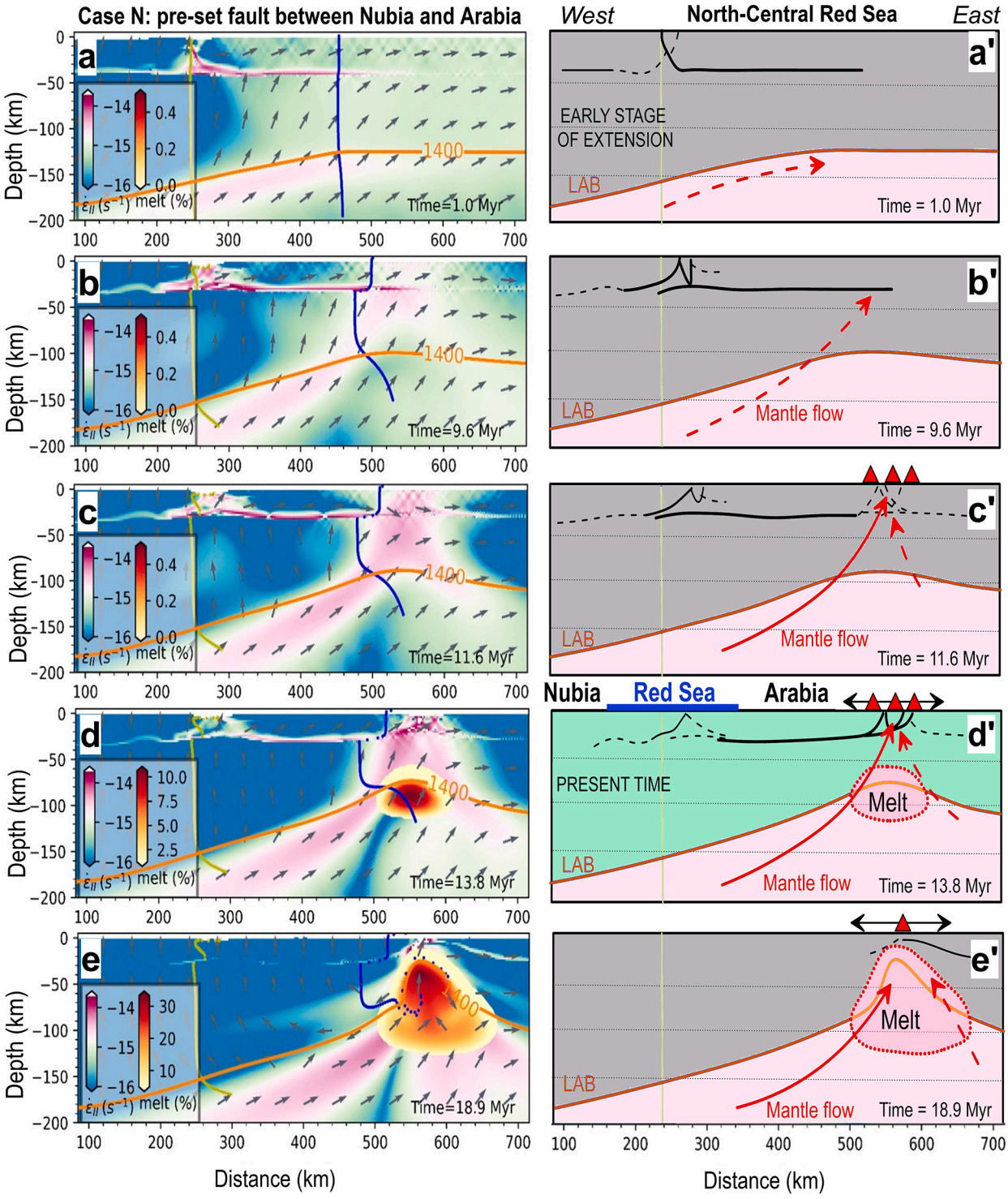

Fig. 8. Case N: Snapshots of strain rate and melt fraction evolution for the north-central Red Sea (left); line-drawings of major model features (right). The pre-set fault is at km 240. Notations as in Fig. 7. (a): A low-angle lithosphere-scale detachment fault is formed at an early stage of extension. (b-d): The weak zone localizes the crustal deformation; white and magenta colors within the crust (black lines in line-drawings) mark the Rea Sea rift graben; lithosphere extension forms a low-angle detachment (subhorizontal lines in a'-d'). (c-d): Lithosphere extension produces a zone of distributed magmatism displaced by ~300 km eastwards from the rift axis. (e-e'): Deformation localizes at the mantle melting region leading to continent breakup. (For interpretation of the references to colour in this figure legend, the reader is referred to the web version of this article.)

the next 1–5 Myr, extensional deformation in the present rift zone will be fully abandoned and transferred to the region of young volcanic provinces in western Arabia, ~300 km eastwards from the Red Sea axis, where the current mantle melt zone is located and all lithosphere extension concentrates. The newly formed lithospheric deformation zone is marked by the system of young grabens, sub-parallel to the north-central Red Sea axis (Zahran et al., 2019) (Fig. 9a), and deformation localizes within a narrow zone typical of continental breakup. Upwards migration of the melt zone to ~50 km depth (Fig. 8e) will cause intensive decompression melting and fast formation of a new spreading

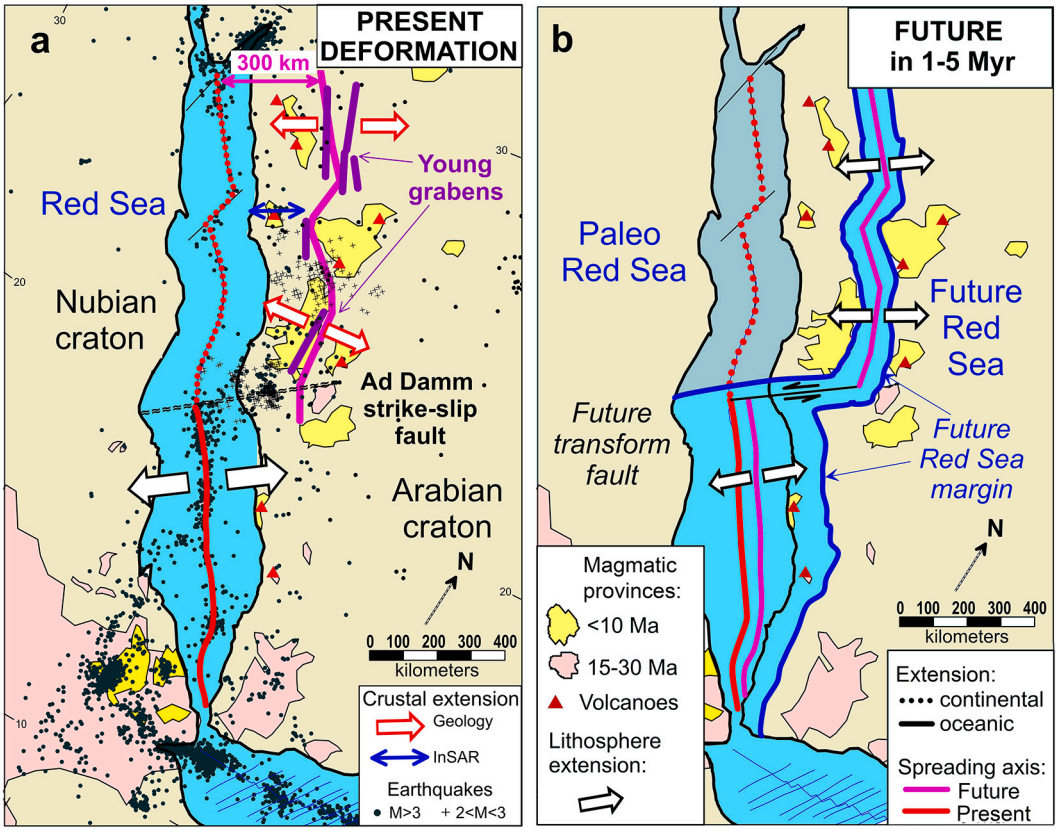

Fig. 9. Evolution of the Red Sea lithosphere extension. (a): Present deformation in the Red Sea region. Seismicity is based on international catalogues (http://www.isc.ac.uk/iscgem/; http://earthquake.usgs.gov/earthquakes/; http://www.emsc-csem.org/Earthquake/) updated for regional 2 < M < 3 onshore events (Zahran et al., 2019). Purple lines – young extensional grabens (Zahran et al., 2019); yellow and pink shading - Cenozoic magmatic provinces (Camp and Roobol, 1992), magenta line follows the Red Sea axis displaced eastwards by 300 km. (b): Future position of the axial zone of lithosphere extension with the formation of a new spreading axis in the north-central Arabia and a transform fault in the Ad Damm fault zone. (For interpretation of the references to colour in this figure legend, the reader is referred to the web version of this article.)

zone across the western Arabian shield, similar to the present southern Red Sea. The melting anomaly has already significantly weakened the Arabian lithosphere and produced young volcanic centres and a NW-SE trending linear belt of young extensional grabens in western Arabia (Fig. 9a). The predicted jump of the extension axis in 1–5 Myr will initiate continental breakup and split the Arabian shield. This process, presently at the final preparation stage, does not require hotspot volcanism at any stage of extension, contrary to previous models for oceans and continents (Kendall et al., 2005; Mittelstaedt et al., 2008).

Our predicted ~300 km rift jump is a new process for continental lithosphere. Similar to oceans, it requires a transform fault to link the spreading axes in the south and north. It is remarkable that a proto-transform fault already exists in the central Red Sea region. The seismically active Ad Damm transpressional shear zone (average width 3 km) extends ~250 km inland in a NE-SW direction (i.e. perpendicular to the Red Sea extensional axis) (Zahran et al., 2019) and marks the transition between the zones of ocean spreading in the south and continental rifting with off-rift magmatism in the north-central Red Sea (Figs. 2, 5, 9a). We propose that the jump of the extensional axis will utilize the Ad Damm fault as the transform fault between the on-going ocean spreading in the southern Red Sea and the incipient mid-ocean ridge which forms in the Arabian shield ~300 km from the present-day rift axis (Fig. 9b).

Our new model for a large-distance jump of extensional axis in continental lithosphere explains geological and geophysical observations at magma-poor continental margins (Whitmarsh et al., 2001) and provides theoretical basis for understanding dynamics and mechanism of the transition from rifting to continental break-up at continental margins not affected by hotspots. Our finding describes a yet unknown process for large-distance jumps of extensional axes in the continental lithosphere and the formation of new spreading centres. Similar jumps may have played an important role in paleotectonics with broad implications for future plate reconstructions.

7. Conclusions

Our model with lithosphere deformation controlled by the location of a pre-extensional crustal-scale weakness zone with respect to the craton margin explains both the north-south and the west-east asymmetries in the evolution of the Red Sea – western Arabia region within a single geodynamic framework. For the north-central Red Sea, the model provides an efficient mechanism for the eastward displacement of the

upper mantle melting zone by 200–400 km from the rift axis by plate-boundary forces, and predicts the future evolution of the north-central Red Sea.

The model predicts that, unless a significant change in plate-boundary forces occurs, extensional deformation in the present rift zone will be fully abandoned during the next 1–5 Myr. The extensional axis will jump to the current mantle melt zone in western Arabia in the region of young volcanic provinces ~300 km eastwards from the Red Sea axis, where all lithosphere extension concentrates and where the incipient mid-ocean ridge forms beneath the Arabian shield.

Data and materials availability

The study is based on the published data, which are available as referenced in the article. The numerical open-source code Underworld2 used for the calculations is available at https://doi.org/10.5281/zenodo.1436039.

Author contributions

IMA developed the idea and wrote the paper with contributions by HY and HT. The numerical modeling was made by HY in discussion with IMA and HT. All authors participated in discussion of the results and their implications. The authors declare no competing interests.

Declaration of Competing Interest

The authors declare that they have no known competing financial interests or personal relationships that could have appeared to influence the work reported in this paper.

Acknowledgments

This study was supported by the grant 92055210 from National Science Foundation of China to HT, the Inge Lehmann's grant of the Royal Danish Academy of Sciences and Letters to IMA, Danish Research Council grant FNU11-104254 to HT, and partially by MOST special funds (China) for GPMR State Key Laboratory (GPMR2019010). This research was undertaken with the assistance of resources and services from the National Computational Infrastructure (NCI), which is supported by the Australian Government. We appreciate comments of Dennis Harry to the early draft of the manuscript, which triggered our interest in future evolutionary scenarios for the Red Sea region. Suggestions of two anonymous reviewers are acknowledged.

Appendix A. Method

A.1. Experimental design

Our regional two-dimensional thermomechanical model with inclusion of melt generation and magmatic processes simulates deformation of the crust and upper mantle under extension in the presence of a pre-existing crustal-scale weakness zone. It leads to continental rift development and incipient ocean spreading. The governing equations of conservation of momentum, mass, and heat (energy) are solved by application of the open-source software Underworld2 (Moresi et al., 2007), which is based on a particle-in-cell finite element algorithm (Moresi et al., 2003). All numerical experiments are run for visco-plastic non-Newtonian rheologies and include creep flow. The modeling accounts for the effects of radioactive heating and mantle melting, assuming generation of basaltic magmas. The 800 km × 400 km numerical model domain is resolved by 400 × 200 quadrilateral elements with linear elements for velocity and constant elements for pressure, that provide a uniformly high model resolution of 2 km. More than 1 million randomly distributed Lagrangian markers (16 markers per cell) are used to track the history of material properties, e.g. density, viscosity and melt fraction. The position of the markers is updated based on the calculated velocity field.

The model evolution caused by a constant outward velocity of 12 mm/yr is specified by the governing equations of conservation of momentum (Eq. (1a)) and mass for incompressible material (Eq. (1b)). The resulting velocity field is coupled with the heat conservation equation (Eq. (1c)) that simulates changes in temperature caused by advection-diffusion heat transfer:

$$\nabla \bullet \sigma - \nabla \mathrm{P} = \rho \mathrm{g} \tag{1a}$$

$$\nabla \bullet \mathrm{u} = 0 \tag{1b}$$

$$\rho C_p \left(\frac{\partial T}{\partial t} + u \bullet \nabla \mathrm{T} \right) = \frac{\partial}{\partial \mathrm{x_i}} \left(\mathrm{k} \frac{\partial \mathrm{T}}{\partial \mathrm{x_i}} \right) + \rho \mathrm{H} \tag{1c}$$

where σ denotes deviatoric stress, P - pressure, ρ - density, g - gravity acceleration, u - velocity, T - temperature, C_p - heat capacity at constant pressure, k - thermal conductivity, H - radioactive heat production. The only heat source is radioactive decay, while heating caused by shear, adiabatic, or melt processes are disregarded.

A.2. Model setup

Laterally, the model extends from the Nubian craton in the west across the Red Sea and into the Arabian craton in the east. Vertically, the model domain includes 5 physical layers: the upper, middle, and lower crust, the lithospheric mantle, and the asthenosphere (Fig. A1). The thickness of each crustal layer is 1/3 of the total crust thickness, in overall agreement with global seismic data (Christensen and Mooney, 1995) and regional seismic data for the Arabian Shield (Mooney et al., 1985; Mechie et al., 1986). The upper and middle crust rheology corresponds to wet quartzite (Ranalli, 1987), whereas the mafic lower crust and the mantle (lithosphere mantle and asthenosphere) rheologies correspond to plagioclase and anhydrous peridotite, respectively (Hirth and Kohlstedt, 2004; Wang et al., 2012). While cratonic lithospheric mantle may have a variable range of water content (Peslier et al., 2010), partial melting of mantle peridotite leads to rock dehydration (Hirth and Kohlstedt, 1996) and strengthening.

The top boundary of the lithosphere between rock surface and air is considered as a free surface; this boundary condition may have a significant effect on lithospheric and mantle dynamics (Kaus and Becker, 2008). To simulate a free surface boundary condition, we add an overlying 20-km-thick "sticky-air" layer (y = 0 to +20 km) represented by a low viscosity (10^{18} Pa·s) and low density (1000 kg/m^3) material (Crameri et al., 2012) (Fig. A1). The evolution of topography is controlled by limiting the elevation lower than the initial model topography, while erosion and sedimentation are not considered and are analysed elsewhere (Yang et al., 2018).

At model time zero the thickness of the continental crust is 40 km in the Nubian shield (model distance x = 0–150 km) and 45 km in the Arabian shield (model distance x = 300–800 km) (Table A1 and Fig. A1). In the Nubian shield, the LAB (lithosphere-asthenosphere boundary) depth of 200 km corresponds to a Paleoproterozoic or a reworked Archean cratonic geotherm of 45–50 mW/m^2, while in the Arabian shield a Neoproterozoic cratonic geotherm of 55–60 mW/m^2 yields the LAB depth of 140 km (Artemieva, 2006), in overall agreement with xenolith geotherms from the Arabia volcanic province (Stern and Johnson, 2010). The difference in lithosphere thickness between the two cratons is important for the model evolution, since the melt zone migrates towards the craton with a thinner lithosphere. We assume a mantle potential temperature of 1400 °C at the LAB; below the LAB mantle temperature increases with an adiabatic gradient of 0.5 K/km.

The two cratonic blocks are separated by a transitional zone with linear ramps at the surface, the Moho, and the LAB (Fig. A1 and Table A1). Within the transitional zone, we introduce a narrow (~6 km wide) crust-cutting rheologically weak zone with plastic strain of 2, which results in a friction coefficient of 0.1 and a cohesion of 5 MPa. The position of the weak zone (dipping at ~75^o towards the Arabian shield) within the transition zone has a determining effect on the lithosphere evolution. We present the results for the two cases which correspond to observations in the north-central and southern Red Sea regions (Figs. 7-8).

A.3. Visco-plastic deformation

The numerical simulations are based on a visco-plastic rheology. Viscous deformation is specified by the power-law dislocation creep:

$$\dot{\varepsilon}_{II} = A\,\sigma_{II}{}^{n} expexp\left(-\frac{E+VP}{RT}\right) \tag{2}$$

where $\dot{\varepsilon}_{II}$ and σ_{II} are the second invariant of strain rate and deviatoric stress, respectively, n is the stress exponent ($n > 1$ for dislocation creep), E - activation energy, V - activation volume, R is the gas constant, A is a material constant, and the effective viscosity is $\frac{\sigma_{II}}{2\dot{\varepsilon}_{II}}$.

For plastic deformation, when stress reaches the transition limit between viscous deformation and plastic failure (Byerlee, 1978), we use the Drucker-Prager pressure-dependent criteria:

$$\sigma_{yield} = \mu P + C \tag{3}$$

where σ_{yield} is the maximum second deviatoric stress invariant, μ is the friction coefficient and C is cohesion. Strain localization is achieved by allowing for a linear strain weakening of friction coefficient (0.6–0.1) and cohesion (20–5 MPa) between plastic strain of 0.5 and 1.5. The composite visco-plastic flow material is modelled with an effective viscosity:

$$\eta_{vp} = min\left(\frac{\sigma_{II}}{2\dot{\varepsilon}_{II}}, \frac{\sigma_{yield}}{2\dot{\varepsilon}_{II}}\right).$$

Its value is limited to the range between 10^{18} Pa·s ("sticky-air" layer and the melt) and 10^{25} Pa·s. Other values of model parameters adopted in the numerical experiments are listed in Table A2.

A.4. Partial melting

The melt function of mantle rocks, implemented for basaltic magmas, describes source regions where partial melting occurs. At model time zero, all mantle rocks are assumed to be melt-depleted. The melting fraction (F) is parameterized as (McKenzie and Bickle, 1988):

$$F\,(T_{ss}) = 0.5 + T_{ss} + \left(T_{ss}^2 - 0.25\right) \times (0.4256 + 2.988T_{ss}) \tag{4}$$

where the supersolidus temperature T_{ss} is defined by the solidus (T_s) and liquidus (T_l) temperatures as:

$$T_{ss} = \frac{T - (T_s + T_l)/2}{T_l - T_s}. \tag{5}$$

We adopt $T_s = 1085.7 + 132.9P - 5.1P^2$ and $T_l = 1475.0 + 80.0P - 3.2P^2$ based on experimental relations with T expressed in °C and P in GPa (Katz et al., 2003). Once the material temperature is higher than the solidus temperature, the material is changed to melt material, i.e. melt fraction $F = 0$ at $T \le T_s$ and $F = 1$ at $T > T_l$. The model does not include the processes of melt extraction and migration, and melt percolation is assumed to be nearly instantaneous (Perchuk et al., 2020). For the melt material, the latent heat and density change is neglected. That means the compositional density for the melt is the same as the source rock density (Table A2). A significant weakening of rock strength happens at a melt fraction of >7% (Rosenberg and Handy, 2005). We adopt viscosity values as for the source rock when the melt fraction is <7%, with a linear viscosity decrease to the lower limit (10^{18} Pa·s) at 30% melt fraction.

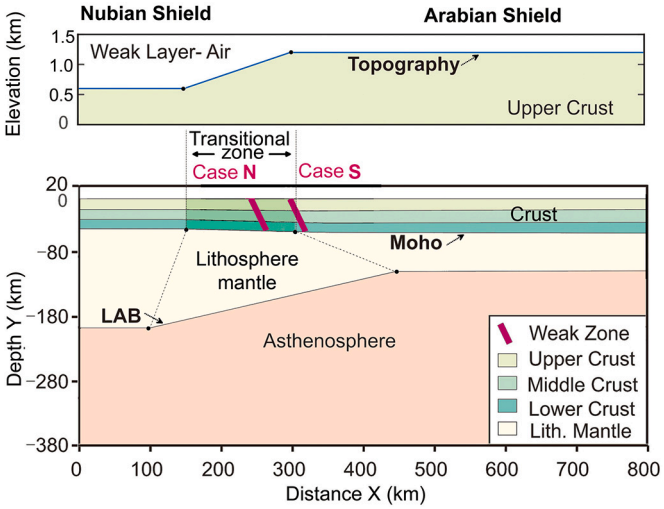

Fig. A1. Design and boundary conditions of the numerical model. Colors indicate materials (crust with three layers, lithospheric mantle, and asthenosphere); LAB is the lithosphere-asthenosphere boundary. Top: A 20 km thick air layer simulates a free surface (Crameri et al., 2012). Bottom: At the start of the extension (time zero), the Nubia and Arabia cratons have different thicknesses of the crust and the lithosphere. Initial crustal thickness and temperature profiles are linearly interpolated in the transitional zone between the two cratons (Table A1). Mantle potential temperature is 1400 °C, and lithosphere extension is caused by a constant outward velocity of Vx = 12 mm/yr, which corresponds to the rate of the central Red Sea opening at 20–22 °N (Chu and Gordon, 1998; ArRajehi et al., 2010). We present two cases for pre-set crustal-scale weakness zones in the transitional zone between the two cratons. The evolution of the model is shown in Figs. 7 and 8. (For interpretation of the references to colour in this figure legend, the reader is referred to the web version of this article.)

Table A1
Model geometry at time zero of the numerical experiments.

Parameter	Nubia (N)	Arabia (A)	N-A transitional zone
Surface elevation	0.6 km	1.2 km	Linear between N-A
Crustal thickness	40 km	45 km	Linear between N-A
Profile distance for crustal thickness	km 0–150	km 300–800	km 150–300
Lithosphere thickness	200 km	140 km	Linear between N-A
Profile distance for lithosphere thickness	km 0–100	km 450–800	km 100–450

Table A2
Physical properties of materials used in the numerical experiments.

Parameter	Symbol (unit)	Upper crust	Middle crust	Lower crust	Mantle**
Material constant	A (MPa^{-n}/s)	3.2×10^{-4}	3.3×10^{-4}	0.01	1.6×10^{4}
Stress exponent	n	2.3	3.2	3.2	3.5
Activation energy	E (kJ/mol)	154	240	240	530
Activation volume	V (cm^3/mol)	0	0	0	18
Density* at 0.1 MPa, 0 °C	ρ_o (kg/m^3)	2700	2850	2950	3300
Heat capacity	Cp (J/kg)	1000	1000	1000	1000
Thermal expansion	α (K^{-1})	3×10^{-5}	3×10^{-5}	3×10^{-5}	3×10^{-5}
Compressibility	β (Pa^{-1})	1×10^{-11}	1×10^{-11}	1×10^{-11}	1×10^{-11}
Thermal conductivity	k (W/mK)	2.5	2.5	2.5	3.5
Radioactive heat production	H_r (μW/m^3)	1.0	0.4	0.1	0.01

Data are from Ranalli (1987); Hirth and Kohlstedt (2004); Wang et al. (2012).
* Density $\rho = \rho_0[1 - \alpha(T - T_0)]\ [1 + \beta(P - P_0)]$, where $T_0 = 298$ K and $P_0 = 0.1$ MPa.
** Lithospheric and asthenospheric mantle.

References

Al-Damegh, K., Sandvol, E., Al-Lazki, A., Barazangi, M., 2004. Regional seismic wave propagation (Lg and Sn) and Pn attenuation in the Arabian Plate and surrounding regions. Geophys. J. Int. 157, 775–795.

Almalki, K.A., Betts, P.G., Ailleres, L., 2015. The Red Sea - 50 years of geological and geophysical research. Earth-Sci. Rev. 147, 109–140.

Al-Saud, M.M., 2008. Seismic characteristics and kinematic models of Makkah and Central Red Sea regions. Arab. J. Geosci. 1, 49–61.

ArRajehi, A., McClusky, S., Reilinger, R., et al., 2010. Geodetic constraints on present-day motion of the Arabian plate. Tectonics 29, TC3011.

Artemieva, I.M., 2006. Global 1°×1° thermal model TC1 for the continental lithosphere: Implications for lithosphere secular evolution. Tectonophysics 416, 245–277.

Artemieva, I.M., Mooney, W.D., 2001. Thermal thickness and evolution of Precambrian lithosphere: a global study. J. Geophys. Res. 106, 16387–16414.

Augustin, N., van der Zwan, F.M., Devey, C.W., et al., 2021. 13 million years of seafloor spreading throughout the Red Sea Basin. Nat. Commun. 12, 2427.

Badri, M., 1990. Crustal structure of Central Saudi Arabia determined from seismic refraction profiling. Tectonophysics 185, 357–374.

Bastow, I.D., Keir, D., Daly, E., 2011. The Ethiopia-Afar geoscientific lithospheric experiment (EAGLE): probing the transition from continental rifting to incipient seafloor spreading. Geol. Soc. Am. Sp. Pap. 478, 51–76.

Benoit, M.H., Nyblade, A.A., VanDecar, J.C., Gurrola, H., 2003. Upper mantle P wave velocity structure and transition zone thickness beneath the Arabian Shield. Geophys. Res. Lett. 30, 1531.

Bialas, R.W., Buck, W.R., 2009. How sediment promotes narrow rifting: Application to the Gulf of California. Tectonics 28, Tc4014.
Bonini, L., Basili, R., Toscani, G., Burrato, P., Seno, S., Valensise, G., 2015. The role of pre-existing discontinuities in the development of extensional faults: an analog modeling perspective. J. Struct. Geol. 74, 145–158.
Bosworth, W., Stockli, D.F., Polat, A., 2016. Early magmatism in the greater Red Sea rift: timing and significance. Can. J. Earth Sci. 53, 1158–1176.
Buck, W.R., 2007. The dynamics of continental break-up and extension. In: Watts, A.B. (Ed.), The Treatise on Geophysics. Crustal and Lithosphere Dynamics, vol. 6, pp. 435–487.
Burke, K., Dewey, J.F., 1973. Plume-generated triple junctions: key indicators in applying plate tectonics to old rocks. J. Geol. 81, 406–433.
Byerlee, J., 1978. Friction of rocks. Pure Appl. Geophys. 116, 615–626.
Camp, V.E., Roobol, M.J., 1992. Upwelling asthenosphere beneath western Arabia and its regional implications. J. Geophys. Res. 97, 15255–15271.
Camp, V.E., Roobol, M.J., Hooper, P.R., 1991. The Arabia continental alkali basalt province: Part II. Evolution of Harrats Khaybar, Ithnayn, and Kura, Kingdom of Saudi Arabia. Geol. Soc. Am. Bull. 103, 363–391.
Chang, S.-J., Merino, M., Van der Lee, S., Stein, S., Stein, C.A., 2011. Mantle flow beneath arabia offset from the opening red sea. Geophys. Res. Lett. 38, L04301. https://doi.org/10.1029/2010gl045852.
Christensen, N.I., Mooney, W.D., 1995. Seismic velocity structure and composition of the continental crust - a global view. J. Geophys. Res. 100, 9761–9788.
Chu, D., Gordon, R.G., 1998. Current plate motions across the Red Sea. Geophys. J. Int. 135, 313–328.
Cloetingh, S., et al., 2013. The Moho in extensional tectonic settings: Insights from thermo-mechanical models. Tectonophysics 609, 558–604.
Cochran, J.R., 2005. Northern Red Sea: Nucleation of an oceanic spreading center within a continental rift. Geochem. Geophys. Geosyst. 6 (3), Q03006.
Coleman, R.G., McGuire, A.V., 1988. Magma systems related to the Red-Sea opening. Tectonophysics 150, 77–100.
Corti, G., 2008. Control of rift obliquity on the evolution and segmentation of the Main Ethiopian rift. Nat. Geosci. 1, 258–262.
Courtillot, V., 1982. Propagating rifts and continental breakup. Tectonics 1, 239–250.
Crameri, F., Schmeling, H., Golabek, G.J., et al., 2012. A comparison of numerical surface topography calculations in geodynamic modelling: an evaluation of the 'sticky air' method. Geophys. J. Int. 189, 38–54.
Deng, C., Gawthorpe, R.L., Finch, E., Fossen, H., 2017. Influence of a pre-existing basement weakness on normal fault growth during oblique extension: Insights from discrete element modeling. J. Struct. Geol. 105, 44–61.
Dunbar, J.A., Sawyer, D.S., 1988. Continental rifting at pre-existing lithospheric weaknesses. Nature 333, 450–452.
Ebinger, C.J., Casey, M., 2001. Continental breakup in magmatic provinces: an Ethiopian example. Geology 29, 527–530.
Ebinger, C.J., Sleep, N.H., 1998. Cenozoic magmatism throughout east Africa resulting from impact of a single plume. Nature 395, 788–791.
Egloff, F., Rihm, R., Makris, J., et al., 1991. Contrasting structural styles of the eastern and western margins of the southern Red Sea: the 1988 SONNE experiment. Tectonophysics 198, 329–353.
El Khrepy, S., Koulakov, I., Gerya, T., et al., 2021. Transition from continental rifting to oceanic spreading in the northern Red Sea area. Sci. Rep. 11, 5594.
El-Isa, Z., Mechie, J., Prodehl, C., Makris, J., Rihm, R., 1987. A crustal structure study of Jordan derived from seismic refraction data. Tectonophysics 138, 235–253.
Elsheikh, A.A., Gao, S.S., Liu, K.H., Mohamed, A.A., Yu, Y., Fat-Helbary, R.E., 2014. Seismic anisotropy and subduction-induced mantle fabrics beneath the Arabian and Nubian Plates adjacent to the Red Sea. Geophys. Res. Lett. 41, 2376–2381.
Ghebreab, W., 1998. Tectonics of the Red Sea region reassessed. Earth-Sci. Rev. 45, 1–44.
Hansen, S., Schwartz, S., Al-Amri, A., Rodgers, A., 2006. Combined plate motion and density-driven flow in the asthenosphere beneath Saudi Arabia: evidence from shear-wave splitting and seismic anisotropy. Geology 34, 869–872.
Hansen, S.E., Rodgers, A.J., Schwartz, S.Y., Al-Amri, A.M.S., 2007. Imaging ruptured lithosphere beneath the Red Sea and Arabian Peninsula. Earth Planet. Sci. Lett. 259, 256–265.
Hirth, G., Kohlstedt, D., 1996. Water in the oceanic upper mantle: implications for rheology, melt extraction and the evolution of the lithosphere. Earth Planet. Sci. Lett. 144, 93–108.
Hirth, G., Kohlstedt, D., 2004. Rheology of the upper mantle and the mantle wedge: a view from the experimentalists. In: Eiler, J. (Ed.), Inside the Subduction Factory, vol. 138. American Geophysical Union, Geophys. Monogr, Washington, DC, pp. 83–105.
Hosny, A., Nyblade, A., 2016. The crustal structure of Egypt and the northern Red Sea region. Tectonophysics 687, 257–267.
Huismans, R., Beaumont, C., 2011. Depth-dependent extension, two-stage breakup and cratonic underplating at rifted margins. Nature 473, 74–U85.
Izzeldin, A.Y., 1987. Seismic, gravity and magnetic surveys in the central part of the Red Sea: their interpretation and implications for the structure and evolution of the Red Sea. Tectonophysics 143, 269–306.
Johnson, P.R., Andresen, A., Collins, A.S., et al., 2011. Late Cryogenian–Ediacaran history of the Arabian–Nubian Shield: A review of depositional, plutonic, structural, and tectonic events in the closing stages of the northern East African Orogen. J. Afr. Earth Sci. 61, 167–232.
Katz, R.F., Spiegelman, M., Langmuir, C.H., 2003. A new parameterization of hydrous mantle melting. Geochem. Geophys. Geosyst. 4.
Kaus, B.J.P., Becker, T.W., 2008. A numerical study on the effects of surface boundary condition and rheology on slab dynamics. Geology 34, 893–896.
Kaviani, A., Paul, A., Moradi, A., et al., 2020. Crustal and uppermost mantle shear wave velocity structure beneath the Middle East from surface wave tomography. Geophys. J. Int. 221 (2), 1349–1365.
Kendall, J.M., Stuart, G.W., Ebinger, C.J., Bastow, I.D., Keir, D., 2005. Magma-assisted rifting in Ethiopia. Nature 433, 146–148.
Koptev, A., Gerya, T., Calais, E., Leroy, S., Burov, E., 2018. Afar triple junction triggered by plume-assisted bidirectional continental break-up. Sci. Rep. 8, 1–7.
Koulakov, I., Burov, E., Cloetingh, S., et al., 2016. Evidence for anomalous mantle upwelling beneath the Arabian Platform from travel time tomography inversion. Tectonophys. 667, 176–188.
KRISP Working Party, 1991. Large scale variation in lithospheric structure along and across the Kenya Rift. Nature 354, 223–227.
Liao, J., Gerya, T., 2015. From continental rifting to seafloor spreading: insight from 3D thermo-mechanical modeling. Gondwana Res. 28, 1329–1343.
Lizarralde, D., Axen, G.J., Brown, H.E., et al., 2007. Variation in styles of rifting in the gulf of California. Nature 448 (7152), 466–469. https://doi.org/10.1038/nature06035.
Makris, J., Rihm, R., 1991. Shear-controlled evolution of the Red Sea: pull apart model. Tectonophysics 198, 441–466.
Makris, J., Allam, A., Mokhtar, T., et al., 1983. Crustal structure in the north-western region of the Arabian shield and its transition to the Red Sea. Bull. Faculty Earth Sci. King Abdulaziz Univ. 6, 435–447.
McGuire, A.V., Bohannon, R.G., 1989. Timing of mantle upwelling: evidence for a passive origin for the Red Sea rift. J. Geophys. Res. 94, 1677–1682.
McKenzie, D., Bickle, M.J., 1988. The volume and composition of melt generated by extension of the lithosphere. J. Petrol. 29, 625–679.
McQuarrie, N., Stock, J.M., Verdel, C., Wernicke, B.P., 2003. Cenozoic evolution of Neotethys and implications for the causes of plate motions. Geophys. Res. Lett. 30, 2036.
Mechie, J., Prodehl, C., Koptschalitsch, G., 1986. Ray–path interpretation of the crustal structure beneath Saudi Arabia. Tectonophysics 131, 333–352.
Mechie, J., Ben-Avraham, Z., Weber, M.H., et al., 2013. The distribution of Moho depths beneath the Arabian plate and margins. Tectonophysics 609, 234–249.
Mittelstaedt, E., Ito, G., Behn, M.D., 2008. Mid-ocean ridge jumps associated with hotspot magmatism. Earth Planet. Sci. Lett. 266, 256–270.
Molnar, N., Cruden, A., Betts, P., 2020. The role of inherited crustal and lithospheric architecture during the evolution of the Red Sea: Insights from three dimensional analogue experiments. Earth Planet. Sci. Lett. 544, 116377.
Mooney, W.D., Gettings, M.E., Blank, H.R., Healy, J.H., 1985. Saudi Arabian seismic-refraction profile: a traveltime interpretation of crustal and upper mantle structure. Tectonophysics 111, 173–246.
Moresi, L., Dufour, F., Mühlhaus, H.B., 2003. A Lagrangian integration point finite element method for large deformation modeling of viscoelastic geomaterials. J. Computat. Physics 184, 476–497.
Moresi, L., Quenette, S., Lemiale, V., et al., 2007. Computational approaches to studying non-linear dynamics of the crust and mantle. Physics of the Earth and Planetary Interiors 163, 69–82.
Morley, C.K., 1989. Extension, detachments, and sedimentation in continental rifts (with particular reference to East Africa). Tectonics 8, 1175–1192.
Osagiede, E.E., Rosenau, M., Rotevatn, A., et al., 2021. Influence of zones of pre-existing crustal weakness on strain localization and partitioning during rifting: Insights from analog modeling using high-resolution 3D digital image correlation. Tectonics 40, e2021TC006970.
Pallister, J.S., McCausland, W.A., Jónsson, S., et al., 2010. Broad accommodation of rift-related extension recorded by dyke intrusion in Saudi Arabia. Nat. Geosci. 3, 705–712.
Park, Y., Nyblade, A.A., Rodgers, A.J., Al-Amri, A., 2007. Upper mantle structure beneath the Arabian Peninsula and northern Red Sea from teleseismic body wave tomography: Implications for the origin of Cenozoic uplift and volcanism in the Arabian Shield. Geochem. Geophys. Geosyst. 8, Q06021.
Perchuk, A.L., Gerya, T.V., Zakharov, V.S., Griffin, W.L., 2020. Building cratonic keels in Precambrian plate tectonics. Nature 586, 395–401.
Peslier, A.H., Woodland, A.B., Bell, D.R., Lazarov, M., 2010. Olivine water contents in the continental lithosphere and the longevity of cratons. Nature 467, 78–81.
Petrunin, A.G., Kaban, M.K., El Khrepy, S., Al-Arifi, N., 2020. Mantle convection patterns reveal the mechanism of the Red Sea rifting. Tectonics 39, E2019TC00582.
Ranalli, G., 1987. Rheology of the Earth. Allen and Unwin, Boston, USA, p. 366.
Reilinger, R., McClusky, S., 2011. Nubia-Arabia-Eurasia plate motions and the dynamics of Mediterranean and Middle East tectonics. Geophys. J. Int. 186, 971–979.
Rosenberg, C.L., Handy, M.R., 2005. Experimental deformation of partially melted granite revisited: implications for the continental crust. J. Metamorph. Geol. 23, 19–28.
Sandvol, E., Seber, D., Barazangi, M., Vernon, F.L., Mellors, R., 1998. Lithospheric seismic velocity discontinuities beneath the Arabian Shield. Geophys. Res. Lett. 25, 2873–2876.
Schaeffer, A.J., Lebedev, S., 2013. Global shear speed structure of the upper mantle and transition zone. Geophys. J. Int. 194, 417–449.
Schettino, A., Macchiavelli, C., Pierantoni, P.P., Zanoni, D., Rasul, N., 2016. Recent kinematics of the tectonic plates surrounding the Red Sea and Gulf of Aden. Geophys. J. Int. 207, 457–480.
Stern, R.J., Johnson, P., 2010. Continental lithosphere of the Arabian Plate: a geologic, petrologic, and geophysical synthesis. Earth Sci. Rev. 101, 29–67.
Tang, Z., Julià, J., Zahran, H., Mai, P.M., 2016. The lithospheric shear-wave velocity structure of Saudi Arabia: Young volcanism in an old shield. Tectonophys 680, 8–27.
Thybo, H., Youssof, M., Artemieva, I.M., 2019. Southern Africa crustal anisotropy reveals coupled crust-mantle evolution for over 2 billion years. Nat. Comm. 10, 5445.

Tkalčić, H., Pasyanos, M.E., Rodgers, A.J., et al., 2006. A multistep approach for joint modeling of surface wave dispersion and teleseismic receiver functions: Implications for lithospheric structure of the Arabian Peninsula. J. Geophys. Res. 111, B11311.
Van Wijk, J., 2005. Role of weak zone orientation in continental lithosphere extension. Geophys. Res. Lett. 32, L02303.
Voggenreiter, W., Hötzl, H., Mechie, J., 1988. Low-angle detachment origin for the Red Sea Rift System? Tectonophysics 150, 51–75.
Wang, Y.F., Zhang, J.F., Jin, Z.M., Green, H.W., 2012. Mafic granulite rheology: Implications for a weak continental lower crust. Earth Planet. Sci. Lett. 353, 99–107.
Whitmarsh, R.B., Manatschal, G., Minshull, T.A., 2001. Evolution of magma-poor continental margins from rifting to seafloor spreading. Nature 413, 150–154.
Wolfenden, E., Ebinger, C., Yirgu, G., Renne, P.R., Kelley, S.P., 2005. Evolution of a volcanic rifted margin: southern Red Sea, Ethiopia. Geol. Soc. Am. Bull. 117, 846–864.
Wright, T.J., Sigmundsson, F., Pagli, C., et al., 2012. Geophysical constraints on the dynamics of spreading centres from rifting episodes on land. Nat. Geosci. 5, 242–250.
Yang, H., Chemia, Z., Artemieva, I.M., Thybo, H., 2018. Control on off-rift magmatism: a case study of the Baikal Rift Zone. Earth Planet. Sci. Lett. 482, 501–509.
Yao, Z., Mooney, W.D., Zahran, H.M., Youssef, S.E.-H., 2017. Upper mantle velocity structure beneath the Arabian shield from Rayleigh surface wave tomography and its implications. J. Geophys. Res. 122, 6552–6568.
Zahran, H.M., Sokolov, V., El-Hadidy, S., 2019. Deterministic seismic hazard assessment for the Makkah region, western Saudi Arabia. Arab. J. Geosci. 12. Art. No. 476.